Artificial Nociceptor Using 2D MoS₂ Threshold Switching Memristor

Durjoy Dev, Student Member, IEEE, Mashiyat S. Shawkat, Adithi Krishnaprasad, Yeonwoong Jung, and Tania Roy, Member, IEEE

Abstract— An artificial nociceptor realized with a single 2D MoS₂-based memristor device is demonstrated in this work. The threshold switching memristor (TSM) device exhibits volatile resistance switching characteristics with low threshold voltage and a high ON-OFF ratio of 10⁶. The Au/MoS₂/Ag TSM device imitates a nociceptor, a special receptor of a sensory neuron that can detect noxious stimulus and transfer the signal to the central nervous system for preventive actions. The single device exhibits all key features of nociceptors including threshold, relaxation, "no adaptation" and sensitization phenomena of allodynia and hyperalgesia depending on the strength, duration, and repetition of the external stimuli. This work indicates applicability of this device in artificial sensory alarm systems for humanoid robots.

Index Terms—2D material, Humanoid robot, MoS₂, Nociceptor

I. INTRODUCTION

THE application of humanoid robots is expanding from I mere research and entertainment platforms sophisticated jobs in industry, battlefield, disaster relief, and space mission [1]-[4]. The sensory system of humanoid robots needs to be responsive to undesirable pressure, external force, mechanical stress, temperature and toxic gas to function efficiently, thereby increasing the robot's lifetime. Fig. 1(a) illustrates the function of a biological nociceptor. The peripheral terminal of the nociceptor receives noxious stimuli and generates a biochemical signal depending on the intensity, duration and recurrence of the stimuli to alert the central nervous system about potential danger [5], [6]. Unlike any other sensory receptor, the nociceptor shows "no adaptation" to noxious stimuli by sustaining its sensitivity to frequently experienced noxious stimuli. To protect an injured area, the nociceptor enhances its sensitivity by reducing its threshold for generating signals (allodynia) and by intensifying its signals (hyperalgesia) [7], [8]. Mimicking such a highly complex nociceptor system with traditional complementary metal oxide semiconductor (CMOS) based sensors would require elaborate circuitry and be power-extensive [9], [10]. Recently, oxidebased memristors have been used to emulate the biological function of the nociceptor. [5], [11], [12]. Most of these reports

This work is supported by the NSF CAREER Award under grant NSF-ECCS-1845331. (Corresponding author: Tania Roy)

Durjoy Dev, Adithi Krishnaprasad, Mashiyat S. Shawkat, Yeonwoong Jung, and Tania Roy are with NanoScience Technology Center, and Department of Electrical and Computer Engineering, University of Central Florida, Orlando FL 32826, USA. (e-mail: tania.roy@ucf.edu)

Yeonwoong Jung, and Tania Roy are with Department of Materials Science and Engineering, University of Central Florida, Orlando FL 32826, USA.

show devices with a high threshold voltage and low ON-OFF ratio and require stimulus voltage pulses with extremely high amplitude and width to emulate the nociceptor actions, which is not suitable for energy-efficient applications [5], [12]. The reliable and robust operation of the nociceptor in a forbidding environment demands a highly stable and energy efficient device. 2D materials-based memristor devices holds promise for such applications since they can withstand higher temperatures compared to conventional oxide-based memristors [11], [13]. MoS₂, a well-studied 2D material offers excellent structural and thermal stability along with the inherent advantages of 2D materials like unique electrical-optical characteristics, high integration density and importantly high elastic moduli required to implement a device on flexible and stretchable substrate specially in harsh environments [13], [17]. 2D materials have been successfully used in non-von Neumann computing paradigms. [14]-[16] The realization of artificial nociceptor using the 2D MoS₂-based single TSM will further the field of 2D neuromorphic devices by allowing a compact, scalable, ultra-light and energy-efficient sensory system, perfect for the large-scale deployment of humanoid robots.

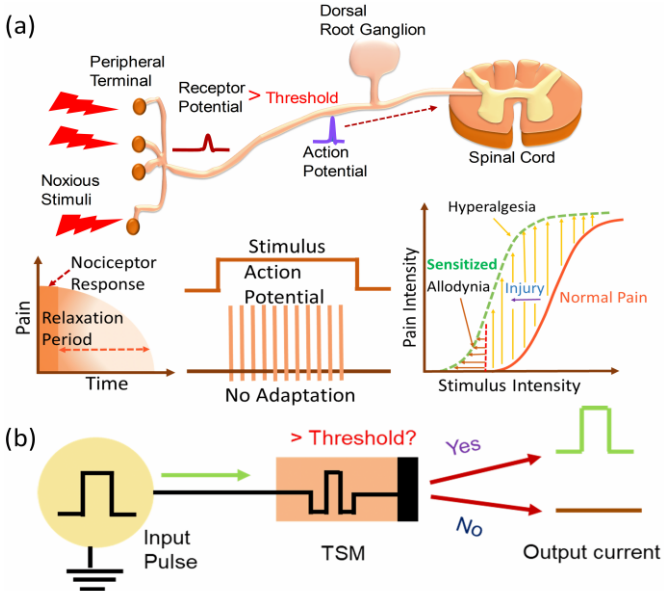


Fig. 1. a) Schematic of biological nociceptor and its key features of threshold, relaxation, "no adaptation" and sensitization. (b) Block diagram of artificial nociceptor circuit realized with 2D MoS₂ TSM device.

In this work, we exploit the volatile switching characteristics of a chemical vapor deposited (CVD) 2D MoS₂-based TSM to realize an artificial nociceptor. The Au/MoS₂/Ag TSM device is connected to an electrical pulsing source to implement the TSM device as an artificial nociceptor (Fig. 1(b)). The device exhibits threshold-driven output response when subjected to

voltage pulse trains of varying amplitude and width. In response to continuous voltage pulses, the TSM device demonstrates "no adaptation" characteristics of the biological nociceptor. When the device is stressed with voltage pulses much higher than its threshold value, the device successfully emulates the sensitization characteristics of the nociceptor and its output resembles the biological nociceptor's allodynia and hyperalgesia characteristics.

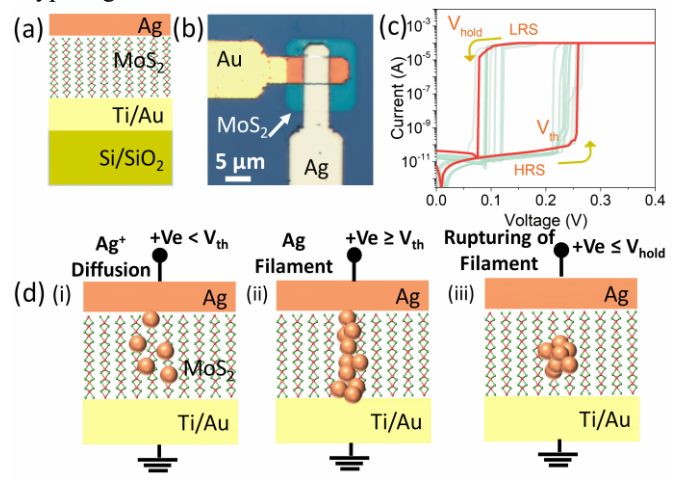


Fig. 2. (a) Schematic of Au/MoS₂/Ag TSM device. (b) Optical image of fabricated Au/MoS₂/Ag TSM device. (c) *I-V* characteristics of the device exhibits threshold switching behavior (9 consecutive cycles shown in faded color). (d) Threshold switching mechanism (i) diffusion of Ag⁺ (ii) Ag filament formation (iii) rupturing of filament.

II. METHODS

The schematic and optical image of the Au/MoS₂/Ag TSM is shown in **Fig. 2(a-b)**. To fabricate an Au/MoS₂/Ag TSM device, Ti/Au (5/100 nm) bottom electrode is patterned and deposited on Si/SiO₂ substrate using standard photolithography and lift-off processes. On top of the bottom electrode, Mo (10 nm) is patterned and deposited by electron beam evaporation. Mo is sulfurized in a low-pressure CVD system at ~780 °C to obtain 2D MoS₂. The top electrode is patterned and Ag/Au (15/40 nm) is deposited by electron beam evaporation. The electrical measurements to characterize the artificial nociceptor are performed on a Micromanipulator probe station (room temperature, in air) using a Keysight B1500A Semiconductor Device Analyzer.

III. RESULTS AND DISCUSSION

Fig. 2(c) demonstrates the DC behavior of the Au/MoS₂/Ag device. The positive bias at the top electrode causes a sharp switching of the TSM device from a high resistance state (HRS) to a low resistance state (LRS) at a threshold voltage (V_{th}) of \sim 0.21-0.26 V, with a high ON-OFF ratio of \sim 10⁶. The device maintains the LRS for positive bias beyond V_{th} . When the voltage is reduced to a value lower than V_{th} (termed as V_{hold} in Fig. 2(c)), the device returns to its HRS and hence loses the programing information. When a positive voltage is applied to the top electrode, a conductive filament is formed due to Ag diffusion from the top to the bottom electrode. The conductive filament causes the device to switch from HRS to LRS (Fig. 2(d)). The removal of the voltage bias causes self-dissolution of the conductive filament due to interfacial energy

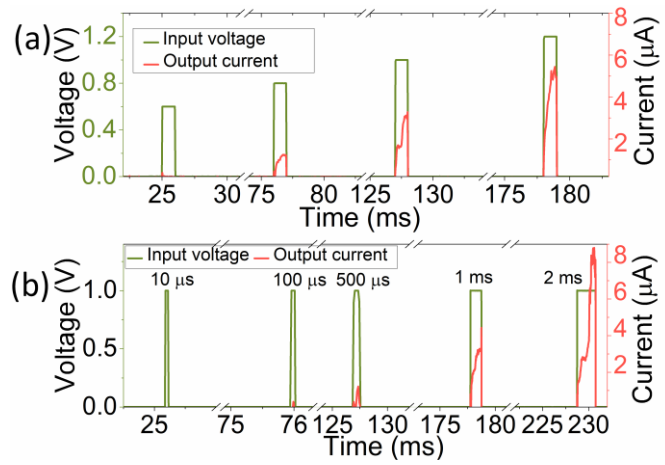


Fig. 3. (a) Output current of artificial nociceptor for input pulse amplitude varying from 0.6 to 1.2 V; pulse width is 1 ms for all pulses. (b) Output current of artificial nociceptor with varying input pulse width of 10 μ s, 100 μ s, 500 μ s, 1ms and 2 ms; pulse amplitude is held constant at 1 V for all pulses.

minimization, hence the device reverts to the HRS state and exhibits the volatile characteristics [18].

The Au/MoS₂/Ag TSM device is connected to an electrical pulsing source (Keysight B1530A WGFMU) to emulate the key features of a biological nociceptor. The TSM device is fed with voltage pulses of increasing amplitude (0.6 V to 1.2 V) with a fixed pulse width of 1 ms. The TSM device turns ON only when the pulse amplitude reaches 0.8 V, as depicted in Fig. 3(a). Following that, the output current increases for increasing pulse amplitude, which implies increased responsivity of the nociceptor with intensified noxious stimuli. Pulses with varying pulse width (10 µs to 2 ms) and a constant pulse amplitude of 1 V are also applied to the device. From Fig. 3(b), it is clear that the device turns ON only after the pulse width reaches 100 µs, and the output current increases for further increase in pulse width, which indicates the elevated sensitiveness of the nociceptor device to the elongated noxious stimulus. These results prove that the TSM device operates only when it reaches a threshold driven by pulse amplitude and pulse width, similar to a biological nociceptor's threshold characteristics.

To investigate the device's response to continuous pulses, a

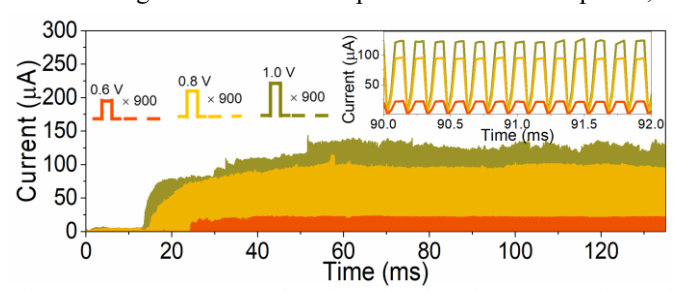


Fig. 4. Output current response for pulse trains of varying pulse amplitudes of $0.6 \, \text{V}$, $0.8 \, \text{V}$ and $1.0 \, \text{V}$; device turns on within a shorter time period for higher voltage amplitudes. Once the device turns on, it maintains the same current level for additional incoming pulses (inset shows the currents for a magnified time scale).

pulse train of varying voltage amplitudes with 100 μs pulse width and 50 μs pulse interval is applied to the device. The continuous stream of input voltage pulses helps in the gradual formation of a conductive filament through MoS₂. Once the filament is formed, it offers a constant electrical path for subsequent pulses. **Fig. 4** shows that while the device turns ON

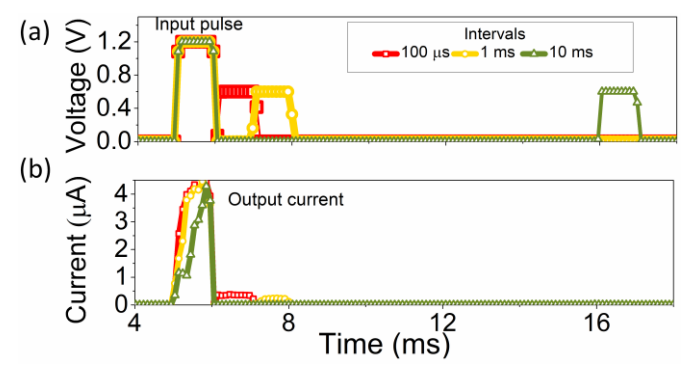


Fig. 5. (a) Input voltage pulse of 1.2~V followed by a 0.6~V pulse with varying interval of $100~\mu s$, 1~ms and 2~ms. (b) Output currents for both input pulses. The device responds to 0.6~V for shorter intervals of $100~\mu s$ and 1~ms between two input pulses. At higher interval of 10~ms, device gets relaxed and does not respond to 0.6~V pulse.

after $\sim\!25$ ms for the 0.6 V input voltage pulses, it turns ON only after $\sim\!15$ ms for the 1 V input voltage pulses. The shorter time required to turn the device ON with higher pulse amplitude implies the faster response of the nociceptor to a stronger stimulus. **Fig. 4** also demonstrates that once the TSM device turns ON, it maintains the same current level for additional pulses without any degradation (plot magnified for a shorter time scale is shown in the inset). This behavior is a clear indication of the "no adaptation" characteristics of a biological nociceptor followed by our device.

After experiencing a noxious stimulus, the biological nociceptor takes a certain period of time to dissipate the response signal, known as the relaxation period. Within this period, the nociceptor responds to noxious stimuli even if they are lower than the threshold value and alerts the central nervous system. To emulate this sensitivity, two pulses of 1.2 V (acting as the noxious stimulus) and 0.6 V (corresponding to a subthreshold stimulus) with 1 ms pulse width are applied at different intervals as shown in Fig. 5(a). Fig. 5(b) shows that, for the low pulse intervals of 100 μs and 1 ms, the TSM device responds to the subthreshold pulse of 0.6 V. As the interval is extended to 10 ms, the device does not respond to the subthreshold pulse of 0.6 V amplitude, which implies that the device is completely relaxed.

For an injured tissue, the nociceptor responds at a lower

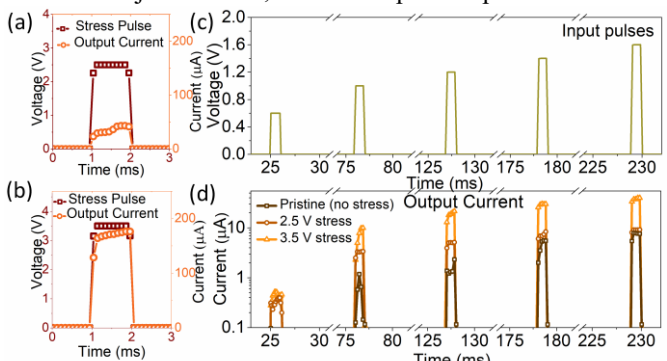


Fig. 6. Device output current vs. time when stressed by applying a single pulse of (a) 2.5 V and (b) 3.5 V. (c) A train of pulses with increasing pulse amplitude of 0.6 V, 1V, 1.2 V and 1.6 V, and 1 ms pulse width is applied to device at pristine condition and stressed condition. (d) Output current in response to pulse train at pristine and injured conditions of 2.5 V stress and 3.5 V stress.

threshold with higher intensity to protect the tissue from further injury. This behavior is known as sensitization. To mimic the

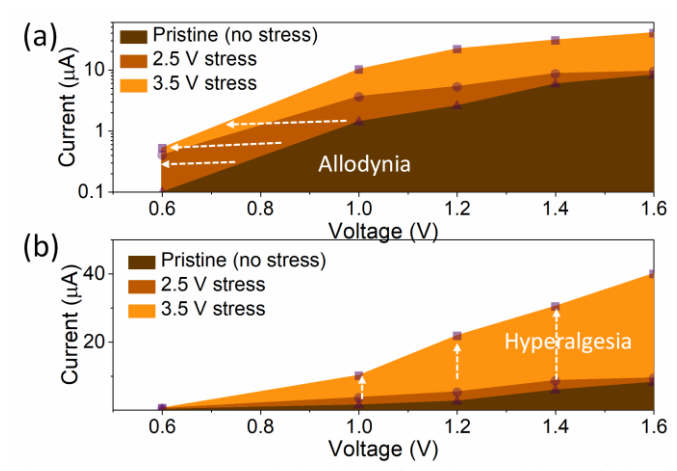


Fig. 7. (a) Output currents obtained for pulse train at pristine and injured condition of Fig. 6 in log scale. The shift of threshold voltage towards lower values implies allodynia characteristics of nociceptor. (b) Output currents obtained for pulse train at pristine and injured condition in linear scale. The increase of current at injured condition implies hyperalgesia characteristics of nociceptor.

injury condition, a pristine TSM device is stressed with pulses of much higher amplitude (first at 2.5 V, then at 3.5 V) than the normal threshold value. Fig. 6(a) and Fig. 6(b) show the output current response of the TSM device in response to single stress pulses of amplitude 2.5 V and 3.5 V respectively. A pulse train of increasing amplitude is applied to the pristine device (no stress) and then after stressing the device at 2.5 V and 3.5 V, as shown in Fig. 6(c). Fig. 6(d) indicates that, while the pristine device shows a threshold at 0.8 V, the threshold reduces to 0.6 V for the stressed conditions. For subsequent voltage pulses of amplitudes 1 V, 1.2 V, 1.4 V and 1.6 V, the stressed devices exhibit higher currents compared to the pristine device. In this case, the stress pulses (2.5 V and 3.5 V) cause the partial formation of a conductive filament through MoS₂ and increase the leakage current of the device, hence the threshold shifts towards the lower voltage and output current increases for the injured device [18]. Fig. 7(a) shows the output currents at pristine and stressed condition in log scale. The shift of the threshold towards lower voltage after stress emulates the allodynia characteristics of the nociceptor. The increasing output current for stressed devices shown in Fig. 7(b) emulates the hyperalgesia nature of the nociceptor. The sensitization property of the nociceptor device would minimize damage to a humanoid robot by being ultra-sensitive following an injury.

IV. CONCLUSION

In conclusion, we have used the threshold switching characteristics of a large area CVD-grown 2D MoS₂ based Au/MoS₂/Ag memristor device to emulate the key features of threshold, "no adaptation", relaxation and sensitization of a biological nociceptor. The device successfully emulates the allodynia and hyperalgesia characteristics of the biological nociceptor when stressed. This work shows the application of lightweight 2D materials in improving the sensory functionalities of a humanoid robot.

REFERENCES

[1] H. Ishiguro, T. Ono, M. Imai, T. Maeda, T. Kanda, and R. Nakatsu, "Robovie: an interactive humanoid robot," *IND ROBOT.*, vol. 28, no. 6, pp. 498-504, 2001, doi:10.1108/01439910110410051.

- [2] K. Tanie, "Humanoid robot and its application possibility." pp. 213-214.doi:10.1109/MFI-2003.2003.1232659.
- [3] K. Kojima, T. Karasawa, T. Kozuki, E. Kuroiwa, S. Yukizaki, S. Iwaishi, T. Ishikawa, R. Koyama, S. Noda, and F. Sugai, "Development of life-sized high-power humanoid robot jaxon for real-world use." pp. 838-843.doi:10.1109/HUMANOIDS.2015.7363459.
- [4] R. O. Ambrose, H. Aldridge, R. S. Askew, R. R. Burridge, W. Bluethmann, M. Diftler, C. Lovchik, D. Magruder, and F. Rehnmark, "Robonaut: NASA's space humanoid," *IEEE Intell. Syst*, vol. 15, no. 4, pp. 57-63, 2000, doi:10.1109/5254.867913.
- [5] Y. Kim, Y. J. Kwon, D. E. Kwon, K. J. Yoon, J. H. Yoon, S. Yoo, H. J. Kim, T. H. Park, J. W. Han, and K. M. Kim, "Nociceptive memristor," *Adv. Mater.*, vol. 30, no. 8, pp. 1704320, 2018, doi:10.1002/adma.201704320.
- [6] A. E. Dubin, and A. Patapoutian, "Nociceptors: the sensors of the pain pathway," *J. Clin. Investig.*, vol. 120, no. 11, pp. 3760-3772, 2010, doi:10.1172/JCI42843.
- [7] A. Latremoliere, and C. Woolf, "Central sensitization: a generator of pain hypersensitivity by central neural plasticity," *J. Pain*, vol. 10, no. 9, pp. 895-926, 2009, doi:10.1016/j.jpain.2009.06.012.
- [8] T. S. Jensen, and N. B. Finnerup, "Allodynia and hyperalgesia in neuropathic pain: clinical manifestations and mechanisms," *The Lancet Neurology*, vol. 13, no. 9, pp. 924-935, 2014, doi:10.1016/S1474-4422(14)70102-4.
- [9] R. S. Dahiya, G. Metta, M. Valle, and G. Sandini, "Tactile sensing—from humans to humanoids," *IEEE Trans. Robot.*, vol. 26, no. 1, pp. 1-20, 2009, doi:10.1109/TRO.2009.2033627.
- [10] R. S. Dahiya, and M. Valle, *Robotic tactile sensing: technologies and system:* Springer Science & Business Media, 2012.
- [11] J. H. Yoon, Z. Wang, K. M. Kim, H. Wu, V. Ravichandran, Q. Xia, C. S. Hwang, and J. J. Yang, "An artificial nociceptor based on a diffusive memristor," *Nat. Commun.*, vol. 9, no. 1, pp. 417, 2018, doi:10.1038/s41467-017-02572-3.
- [12] M. Xiao, D. Shen, M. H. Futscher, B. Ehrler, K. P. Musselman, W. W. Duley, and Y. N. J. A. E. M. Zhou, "Threshold Switching in Single Metal-Oxide Nanobelt Devices Emulating an Artificial Nociceptor," Adv. Electron. Mater., 2019, doi:10.1002/aelm.201900595.
- [13] M. Wang, S. Cai, C. Pan, C. Wang, X. Lian, Y. Zhuo, K. Xu, T. Cao, X. Pan, and B. Wang, "Robust memristors based on layered two-dimensional materials," *Nat. Electron.*, vol. 1, no. 2, pp. 130-136, 2018, doi:10.1038/s41928-018-0021-4.
- [14] S. Das, A. Dodda, and S. Das, "A biomimetic 2D transistor for audiomorphic computing," *Nat. Commun.*, vol. 10, no. 1, pp. 1-10, 2019, doi:10.1038/s41467-019-11381-9.
- [15] A. Sebastian, A. Pannone, S. S. Radhakrishnan, and S. Das, "Gaussian synapses for probabilistic neural networks," *Nat. Commun.*, vol. 10, no. 1, pp. 1-11, 2019, doi:10.1038/s41467-019-12035-6.
- [16] F. Zhang, H. Zhang, S. Krylyuk, C. A. Milligan, Y. Zhu, D. Y. Zemlyanov, L. A. Bendersky, B. P. Burton, A. V. Davydov, and J. Appenzeller, "Electric-field induced structural transition in vertical MoTe 2-and Mo 1–x W x Te 2-based resistive memories," *Nat. Mater.*, vol. 18, no. 1, pp. 55-61, 2019, doi:10.1038/s41563-018-0234-y.
- [17] K. Liu, Q. Yan, M. Chen, W. Fan, Y. Sun, J. Suh, D. Fu, S. Lee, J. Zhou, and S. Tongay, "Elastic properties of chemical-vapor-deposited monolayer MoS2, WS2, and their bilayer heterostructures," *Nano Lett.*, vol. 14, no. 9, pp. 5097-5103, 2014, doi:10.1021/nl501793a.
- [18] D. Dev, A. Krishnaprasad, M. S. Shawkat, Z. He, S. Das, D. Fan, H.-S. Chung, Y. Jung, and T. Roy, "2D MoS2 Based Threshold Switching Memristor For Artificial Neuron," *IEEE Electron Device Lett.*, vol. 41, no. 6, pp. 936-939, 2020, doi:10.1109/LED.2020.2988247.